Virchows Archiv (1994) 425:181–193

ORIGINAL ARTICLE

Matthias Kretzler · Inge Koeppen-Hagemann
Wilhelm Kriz

Podocyte damage is a critical step in the development of glomerulosclerosis in the uninephrectomised-desoxycorticosterone hypertensive rat

Received: 19 January 1994 / Accepted: 14 June 1994

Abstract The progressive renal disease model of chronic uninephrectomy-desoxycorticosterone-trimethylacetate (UNX-DOCA) hypertension is associated with mesangial proliferation as a major disease mechanism. A detailed structural analysis of the alterations in glomerular structure which accompany the development of sclerosis in this model has not been made. Male Munich-Wistar rats underwent UNX, received weekly injections of the aldosterone agonist DOCA and 1% sodium chloride as drinking solution and were compared with sham operated controls (CON). Thirty eight days after onset, UNX animals had an albuminuria of 183±180 mg/day versus 0.38±0.22 mg/day in CON. Kidneys were fixed by total body perfusion and renal tissue processed for light and electron-microscopy. Superficial and deep total glomerular volume increased from 2.18±0.15 (deep: 2.57±0.24) 10^6 μm^3 in CON to 3.98±0.81 (deep: 3.95±0.63) 10^6 μm^3 in UNX. In addition to overall tuft hypertrophy, structural analysis revealed severe destruction of tuft architecture with mesangial expansion and/or capillary ballooning, leading to local tuft enlargements. Podocytes overlying the expanded areas appeared unable to adapt to cover the increased tuft surfaces. They developed severe lesions in cell architecture leading to denudation of glomerular basement membrane (GBM)-areas. "Naked" GBM appears to represent a nidus for hyalinosis, thrombosis and synechia formation, which progresses to segmental sclerosis. In the UNX-DOCA model of chronic glomerular hypertension local mesangial expansion was frequently encountered but no evidence was found that mesangial proliferation and matrix production proceeded to sclerosis. The crucial damage to the glomerulus in this model would appear to be attributable to podocyte failure, with the resultant GBM denudation triggering synechia formation, hyalinosis and ultimately glomerulosclerosis.

M. Kretzler · I. Koeppen-Hagemann · W. Kriz (✉)
Anatomy and Cell Biology Institute I, University of Heidelberg,
Im Neuenheimer Feld 307, D-69120 Heidelberg, Germany

Key words Glomerular epithelial cells
Glomerular hyperperfusion · Uninephrectomy
Mesangial expansion · Synechia

Introduction

Chronic uninephrectomy-desoxycorticosterone-trimethylacetate (UNX-DOCA) hypertension, a model characterized by high intraglomerular pressures [3, 4] has been frequently used to study progressive renal disease. In this model, as in other hypertensive models, it has been widely assumed that mesangial proliferation and matrix deposition represent the major pathological alterations leading to sclerosis. However, a detailed analysis of the structural alterations in other glomerular cell types and their possible role in sclerosis is lacking.

The present study does not address the question why a glomerulus degenerates, it addresses the question how this occurs. Based on a thorough analysis of the structural changes we wanted to define the precise sequence of lesions which finally terminates in sclerosis.

We found two distinctly different damage patterns, suggesting two pathways leading to sclerosis. In the first, obstructive lesions in preglomerular vessels lead to glomerular atrophy. These observations will be described elsewhere. The second type of lesion, associated with glomerular hypertrophy and evidence of elevated glomerular pressures, results in widespread destruction of glomerular architecture developing to glomerular sclerosis.

Surprisingly, in both pathways mechanisms other than mesangial proliferation appear critical for the final degeneration of the glomerulus. In this model the lack of adaptive capacity of the visceral glomerular epithelial cells (podocytes) to the alterations of glomerular architecture seems to be responsible for the irreparable glomerular damage leading to sclerosis.

Materials and methods

Experiments were performed on male Munich-Wistar rats (Ivanovas, Kissleg, Germany) with initial body weights of 150–170 g following the protocol of Dworkin and co-workers [3]. During an adjustment period of 4 days with standard chow (Altromin, Lage, Germany: 19% protein, 0.2% sodium, 0.9% calcium, 1.0% potassium) and freely available tap water the baseline systemic blood pressure of each animal was determined using tail plethysmography [40]. Following this period one group (n=15) underwent UNX, whereas the remaining group (n=10) was sham-operated (CON).

For the following 6 weeks both groups were kept on the same food as before, but UNX rats received 1% sodiumchloride as drinking solution. Additionally, this group received weekly subcutaneous injections of DOCA (45 mg/kg body weight DOC-TMA, Ciba, Basel, Switzerland) starting on the day of nephrectomy. CON rats were given weekly subcutaneous injections of 0.9% carrier solution. Systemic blood pressure and body weight were recorded twice weekly, food and fluid intake on a daily basis.

At the end of the 6 week period the following variables were estimated: sodium, potassium and creatinine concentrations in serum; haematocrit; urinary excretion of sodium, potassium, creatinine and albumin. Electrolyte concentrations in serum and urine were determined by flame photometry. Creatinine was measured with the picric acid reaction. Urinary albumin concentration was estimated by a modified method of Mancini single radial immunodiffusion [20] using an anti-rat albumin antibody in whole lyophilized serum (provided by John Hoyer, Childrens Hospital, University of Philadelphia, USA). Rat serum albumin (fraction V powder, Sigma , St. Louis, USA) was used as standard.

On day 45 in vivo perfusion fixation of the kidneys was carried out as described previously [16]. After anaesthesia with Inactin (100 mg/kg body weight), the abdominal cavity was opened and the kidneys were perfused retrogradely via the abdominal aorta without prior flushing of the vasculature. Perfusion pressure in the perfusing apparatus was 80 mmHg above the last determined systolic blood pressure (190 mmHg in CON and between 220–300 mmHg in UNX) and was maintained for 3 min. The fixative contained 3% glutaraldehyde in 0.1 M cacodylate buffer (pH 7.4) supplemented with 0.08% calcium chloride, 0.5 g/l picric acid and 25 g/l polyvinylpyrrolidon (molecular weight 40000). After perfusion the kidneys were removed immediately and immersed in the same fixative for a maximum of 2 days until further processing.

The right kidney of CON animals and the lower half of the remaining left kidney of UNX rats were processed for light microscopy following standard procedures. After embedding in paraplast, sections of 2 and 4 µm thickness were cut and stained with haematoxylin and eosin.

Tissue for transmission electron microscopy (TEM) was processed in two ways. The classic osmium tetroxide (OsO_4) postfixation technique (including dehydration in a graded series of ethanols) was applied and a modified postfixation and staining technique was used which minimizes treatment with OsO_4 and uses tannic acid as a contrast agent [35]. All tissues were finally embedded in Epon 812 by standard procedures.

Semi-thin sections (1 µm thickness) were cut on a Sorval Porter-Blum MT-2B ultramicrotome and stained with azure II – methylene blue and examined by light microscopy (Polyvar 2, Reichert). Ultrathin sections (grey to silver) were cut with a diamond knife on a Reichert-Jung Ultracut E microtome and placed on formovar-coated copper grids. They were stained in 5% uranyl acetate for 15 min and subsequently in Reynolds lead citrate for 2 min. They were observed under a Philips EM 301 EM.

For scanning EM (SEM) 3 mm thick coronal sections were dried, mounted on aluminum stubs with silver conductive paint, sputter-coated with gold (10 nm), and examined in a Philipscan 500 SEM at 25 kV.

To assess glomerular damage 100 glomeruli of each animal were screened in 4 µm paraffin sections for the following phenomena; focal glomerular sclerosis, adhesions to Bowman's capsule, glomerular atrophy and microaneurysms. The incidence of each was determined. Additionally, sections were screened for the presence of necrotic vascular lesions.

The frequency of different degrees of mesangial expansion was estimated following Dworkin et al. [4]. In a blinded fashion in randomly selected meridional 2 µm sections 100 consecutive glomeruli in each animal were graded according to the estimated relative mesangial area: grade 0: slim mesangial matrix, lobules contain no more than two mesangial cells; grade 1: thin matrix, three or four mesangial cells in one lobule; grade 2: expanded matrix, three or four mesangial cells in every lobule; grade 3: plump matrix, more than four mesangial cells in all lobules. Glomeruli with adhesions, glomerular atrophy or global sclerosis were excluded. Based on this estimation of the degree of mesangial expansion a mesangial expansion score (MES) was calculated for each rat: MES=0×(% grade 0)+1×(% grade 1)+2×(% grade 2)+3×(% grade 3).

Morphometric analysis was carried out with a semiautomatic image analysis system (VIDS IV, Ai Tektron, Düsseldorf, Germany) for the following parameters: glomerular and tuft cross-sectional area and width of capillary necks (distance between two opposite mesangial angles).

Mean total glomerular (VG) and tuft volumes (VT) were determined according to a commonly used procedure first described by Weibel [42]. Surface areas of the total glomeruli (AG; including Bowman's capsule) and glomerular tufts (AT) were determined in 2 µm paraffin sections under direct visualization (magnification 690×) in a blinded fashion. The evaluation was carried out separately for superficial and juxtamedullary glomeruli. Glomeruli situated within 500 µm of the renal capsule were considered to be superficial, and glomeruli within 500 µm of the corticomedullary junction to be juxtamedullary glomeruli. For each rat 100 consecutively encountered superficial, and 100 juxtamedullary glomeruli were analysed. Atrophic glomeruli were excluded from analysis.

VG and VT were calculated according to the formula [42]: VT or $VG=(\beta/k)\ (A)^{3/2}$ where β=1.38 (the shape coefficient), k=1.1 (the size distribution coefficient for spheres) and A=mean AG or AT. Because paraffin embedding causes shrinkage of the renal tissue by roughly 48% [7] reported values of glomerular and tuft volumes are corrected for shrinkage.

The width of capillary necks was determined as the distance between two opposing mesangial angles in relation to the full capillary circumference (for illustration see arrows in Fig. 4a) was obtained from TEM of central sections of superficial glomeruli. Glomeruli with atrophic changes or microaneurysms were excluded from analysis. Printed glomerular profiles on micrographs at a final magnification of ×1850 were used for measurement. To facilitate tracing of the capillary circumference and the capillary neck with the digitizer mouse, the course of these structures was outlined in advance with a marking pen on TEM photos. The relative length of the capillary neck was calculated by dividing the length of the capillary neck by the full circumference of the capillary [39].

The glomeruli were divided into three subgroups according to the degree of ME. The mean group value was determined in the following stepwise fashion: the mean diameter of the capillary necks for each glomerulus was calculated, then the median value for each animal and finally the group mean value was determined. The groups comprised: group 1: CON: ME grade 0–1, ten rats with three glomeruli per animal; total 30 glomeruli with 1442 capillaries; group 2: UNX: ME grade 0–1, 11 rats with two or three glomeruli per animal; total 30 glomeruli with 1683 capillaries; group 3: UNX: ME grade 2–3, 11 rats with two or three glomeruli per animal; total 31 glomeruli with 1662 capillaries.

Results are reported as mean±standard deviation (SD). Differences between the two groups were tested with the unpaired Student's t-test (functional data, glomerular size) or with the Mann-Whitney-Wilcoxon test (MES, width of capillary necks). Differences between subgroups were tested with the paired Student's t-test (glomerular size, superficial vs deep) or with the Wilcoxon matched pair test (width of capillary necks). Linear regression analysis was used to examine the relation between albuminuria and MES. All statistical analyses were performed with the SPSS

Table 1 Whole animal data (values are expressed as average±standard deviation, *Con* controls, *UNX* uninephrectomy)

* $P<0.05$, ** $P<0.001$, comparison between UNX and CON rats within the same time group

	Body weight		Blood pressure		Kidney weight (g)
	initial (g)	final (g)	initial (mmHg)	final (mmHg)	
CON (n=10)	161 ±9	285 ±28	111 ±10	112 ±10	2.28 ±0.18
UNX (n=12)	162 ±7	252* ±29	112 ±11	181** ±13	2.28 ±0.29

Table 2 Serum (*S*) and urinary (*U*) values (*Hct* haematocrit, *Crea* creatinin, *Alb* albumin, K^+ potassium, Na^+ sodium)

The small and varying numbers for "n" in serum values result from the fact that it has not been possible in all animals to obtain sufficient blood for analysis

	S_{Na}^+ (mmol/l)	S_k^+ (mmol/l)	Hct (%)	S_{Crea} (mg/dl)	U_{Alb} (mg/24 h)
CON	142.8 ±3.6 (n=8)	3.92 ±0.31 (n=8)	45.2 ±2.6 (n=5)	0.45 ±0.03 (n=6)	0.38 ±0.22 (n=10)
UNX	145.1 ±5.0 (n=6)	2.66** ±0.25 (n=6)	43.3 ±1.2 (n=6)	0.60* ±0.13 (n=6)	183** ±180 (n=12)

analysis program (Chicago, Illinois, USA). Statistical significance was defined as $P<0.05$.

The term "glomerulosclerosis" is used in the definition given by Rennke [32] as the glomerular lesion which "consists of global or segmental collapse of the capillaries with disappearance of the cellular elements and microvascular lumina, entrapment of foamy macrophages, cellular debris and hyaline material, also known as hyalinosis and adhesion of the tuft to Bowman's capsule by synechia".

Results

Functional data

UNX, DOCA-administration and a high sodium intake induced marked systolic hypertension, hypokalaemia and albuminuria, leading to "malignant" form of hypertension in 7 out of 15 animals. Towards the end of the experiment they showed a loss of body weight and developed neurological abnormalities including hemiparesis. Three of these severely affected animals died in the last week of the experiment. The four surviving animals exhibited fibrinoid necrosis of preglomerular vessels.

Data on the changes of body weight, kidney weight, systolic blood pressure, urinary albumin excretion and serum values are given in Tables 1 and 2. All animals gained weight steadily throughout the first 4 weeks of the study; four rats of the UNX group lost weight towards the end of the experiment. The weight of the single kidney in UNX rats (2.28±0.29 g) reached the weight of the two kidneys in CON animals (2.28±0.18 g).

The raise in blood pressure in the UNX rats became significant 3 weeks after UNX ($P<0.001$). As can be seen in Fig. 1, a plateau was reached after 4–5 weeks at a systolic blood pressure of about 180 mmHg. The CON group showed no change in blood pressure. Urinary albumin excretion measured at the end of the experiment was significantly higher in UNX compared to CON (see Table 2).

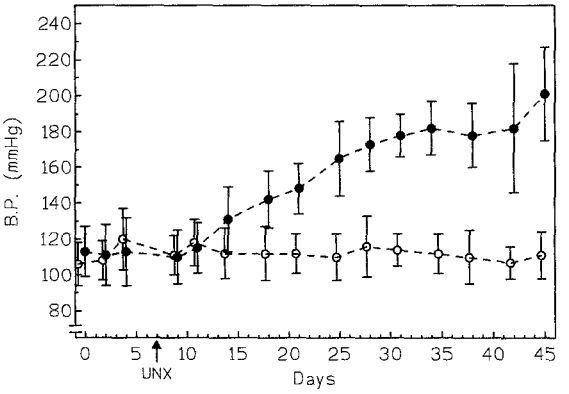

Fig. 1 Blood pressure in uninephrectomy (UNX) and control (CON) animals. Mean±SD are shown. *Filled circles* UNX-animals, *open circles* CON-animals, *UNX* start of experiment

Table 3 Mesangial expansion score (MES)

	MF				MES
	0 (%)	1 (%)	2 (%)	3 (%)	
CON (n=10)	25.2 ±14.6	61.8 ±6.2	12.3 ±10.3	0.7 ±0.9	0.89 ±0.23
UNX (n=12)	7.7 ±7.7	40.0 ±17.4	31.5 ±7.3	21.3 ±16.6	1.67** ±0.46

Incidence of glomerular lesions

The incidence of glomerular lesions was determined in paraffin sections; 100 glomerular profiles in each UNX rat were evaluated. We found for glomerular atrophy an incidence of 7.92% (range 1–20%), for glomerular sclerosis 5.08% (range 0–14%), for adhesions to Bowman's capsule 5.93% (range 2–16%), for glomerular microaneurysms, 1.17% (range 1–3%). Such lesions were not observed in CON rats.

Table 4 Glomerular hypertrophy (*BC* Bowman's capsule, *sup* superficial, *jux* juxtamedullary)

Values are expressed as average ± SD; $^{**}P<0.001$, comparison between CON and UNX; $^{++}P<0.001$ comparison between sup. and jux. volumes in CON; no significant differences between sup. and jux. volumes in UNX

	BC volume ($\times 10^6$ µm^3)		Tuft volume ($\times 10^6$ µm^3)		Tuft/BC volume	
	sup	jux	sup	jux	sup	jux
CON (n=10)	2.18^{++} ±0.15	2.57 ±0.24	1.40^{++} ±0.10	1.61 ±0.13	0.64 ±0.02	0.63 ±0.03
UNX (n=10)	3.98** ±0.81	3.95** ±0.63	2.09** ±0.45	1.96** ±0.26	0.53** ±0.05	0.50** ±0.05

Mesangial expansion grading and scoring

Using the semi-quantitative scoring system of Dworkin et al. [4] different degrees of ME, ranging from mild to marked, were found in all UNX kidneys (Table 3). In both CON and UNX, most glomeruli were assigned to grade 1 ME with relative frequencies of 62% in COn and 40% in UNX. Only 13% of CON glomeruli showed grade 2 or 3 ME, compared to more than 50% of UNX glomeruli.

These findings resulted in an MES which was significantly higher in UNX (1.67) than in CON (0.89, $P<0.001$). Albuminuria was positively correlated to MES (r=0.88).

Glomerular hypertrophy

Both total and VT were greater in the UNX group than in CON for both superficial and deep glomeruli. As can be seen from Table 4, UNX led to an increase in VG (82% in superficial, 52% in deep glomeruli) as well as in VT (49% and 22%, respectively). Thus, the glomerular tuft occupies a greater part of the total glomerular volume in CON (64% and 63%, respectively for superficial and deep glomeruli) than in UNX (53% and 50%).

Widths of capillary necks

Determination of the capillary-mesangial interface at the capillary neck revealed a greater neck width in UNX animals than in CON ($P<0.01$). Moreover, the value increased in UNX along with an increase in mesangial expansion from 24% at an ME of 0–1 to 33% at a ME of 2–3 ($P<0.01$). In CON the capillary neck width amounted to 20%.

Analysis of structural lesions

Structural glomerular lesions were manifold and heterogeneous. The inter-animal variability in the degree of glomerular damage was remarkable, with some animals showing only a few damaged glomeruli while others had severe lesions in the majority of glomeruli. The lesions were distributed focally and range from mild to severe including glomerulosclerosis.

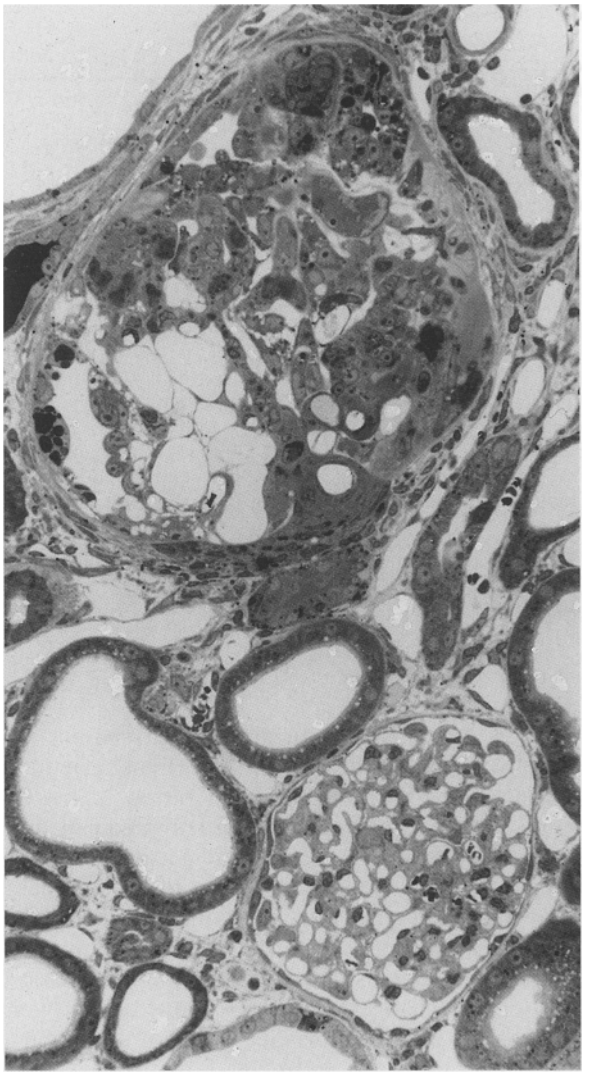

Fig. 2 Glomerular destruction versus glomerular atrophy. Light microscopy of two neighbouring glomerular profiles showing the two different damage patterns. The upper profile exhibits the final stage of the destructive pathway with a massively enlarged and partially sclerosed glomerulus. The lower profile demonstrates the features of the atrophic pathway. A small shrunken glomerulus is seen representing an intermediate stage; the final stage is an even smaller cell ball without any open spaces

The different lesions do not appear to arise from a single pathogenetic mechanism. Two pathways could clearly be distinguished. In addition to a hypertrophic destructive pathway terminating in glomerulosclerosis, glomerular

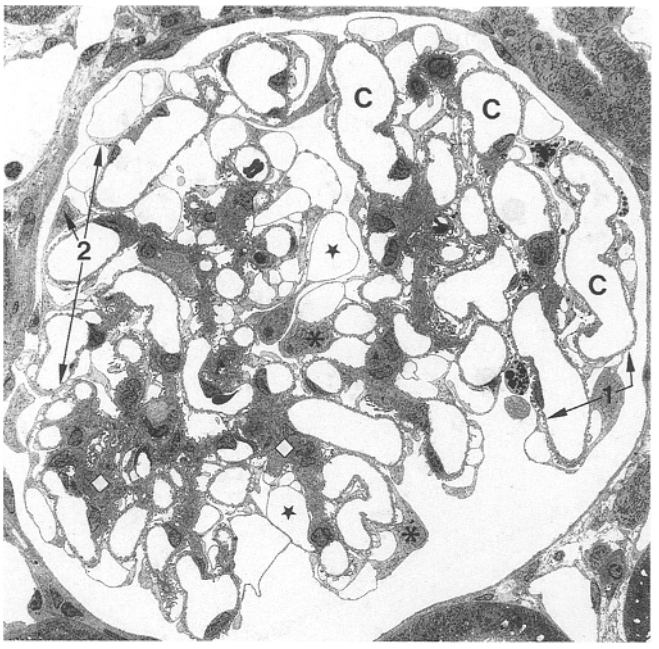

Fig. 3 Glomerulus showing various aspects of tuft destruction. Transmission electron micrograph (TEM) shows lobular expansion either in areas of capillary ballooning (*C*) or in areas of mesangial expansion and proliferation (*quadrangles*). Lobular expansion is associated with a massive hypertrophy of podocytes (*asterisks*); each podocyte serves large capillary surfaces (outlined by *arrows* for podocytes *1* and *2*). Podocytes exhibit extensive maladaptive changes including intracellular protein droplets and multiple pseudocysts (*stars*), ×650

atrophy was found (Fig. 2) and these glomeruli were regularly associated with obstructive lesions in preglomerular vessels. They were found predominantly in the four surviving animals with "malignant" hypertension. These observations will be published elsewhere.

The destructive lesions observed in hypertrophied glomeruli (Fig. 3) consisted of local mesangial expansion, generally associated with small capillary profiles. In contrast, other areas of the tuft frequently exhibited conspicuously large capillaries occurring alone or in small groups. Both types of changes sometimes occurred together in the same lobule. Both lesions were commonly accompanied by degenerative changes in podocytes, which appear to be secondary to mesangial expansion and/or capillary ballooning. Most severely damaged glomeruli showed different stages in the development of glomerulosclerosis.

1. Mesangial expansion

Three types of mesangial changes were seen, all of which could be associated with an increase in mesangial area. First, the mesangial cells appeared hypertrophied, with more extensive branching into cell processes stuffed with a dense assembly of microfilaments. The hypertrophic changes were most clearly seen in juxtacapillary cell processes at the capillary necks (Fig. 4). The necks

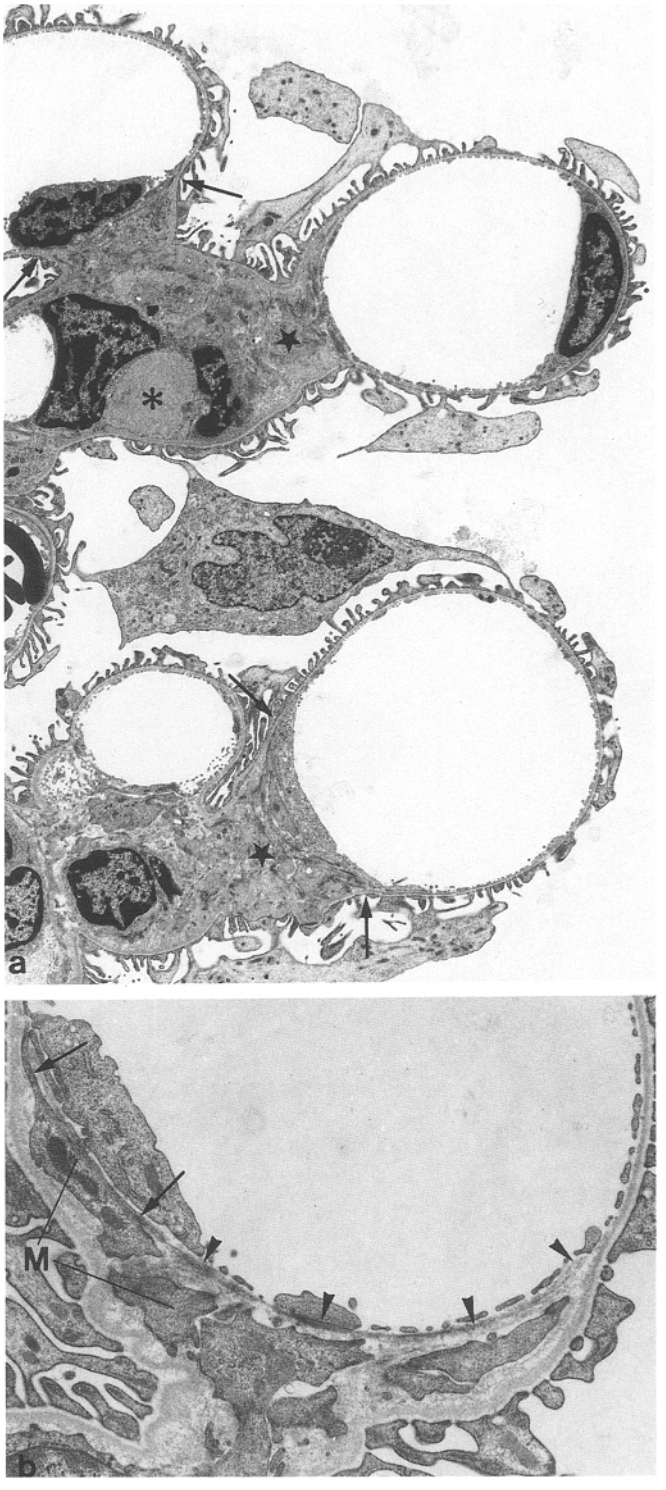

Fig. 4a, b Mesangial hypertrophy. These TEMs show (**a**) subdivision of a lobule showing mesangial hypertrophy in parallel to mesangial lesions. Mesangial processes are densely packed with microfilaments (*stars*), most prominent in the juxtacapillary processes extending to the mesangial angles (*arrows*). Simultaneously, open fluid filled spaces are encountered within the mesangium (*asterisks*), indicating local mesangial failure. **b** Widened capillary neck, stabilized by mesangial processes (*M*) which contain dense bundles of microfilaments (*arrows*); extracellular microfibrils (*arrowheads*) are also prominent (**a**) ×3200, (**b**) ×12100

Fig. 5 Acute mesangial expansion. This TEM shows subdivision of a lobule with several expanded mesangial areas (*1, 2, 3*). At these sites, mesangial cell processes (*arrows*) are seen, which have obviously lost their connections to the glomerular basement membrane (GBM). The widened mesangial spaces appear either empty (*2*), or are filled with granular material of varying density (*1, 3*). ×3200

Fig. 6 Solidified mesangial expansion. TEM of a dilated mesangial axis with multiple extensively branching mesangial cell processes (*asterisks*) in a dense matrix. The outpocketings are filled with matrix and mesangial processes reaffixing the GBM to the mesangium (*arrows*). Podocytes display maladaptive changes including intracellular droplets (*PD*) and "fusion" of foot processes (*FF*). ×4500

were generally widened (convincingly shown by the morphometric results; see above); the mesangial connections which bridge the two opposing mesangial angles appeared strengthened. Second, mesangial expansion was frequently seen as a local widening of the mesangial space filled with an amorphous fluid. Small outpocketings of the perimesangial GBM were encountered. These bulged into Bowman's space locally and lead to an asymmetrical dilation of the mesangium (Fig. 4). In more extensive cases, large fluid filled spaces along the mesangial axes were seen (Fig. 5). Disconnections of mesangial cell processes and retractions from the GBM were frequently encountered, whereas other connections appeared to be stretched out with small bundles of microfibrils maintaining some contact with the GBM (Fig. 5). Third, expanded mesangial areas were seen filled with profiles of mesangial cells and cell processes in a compact solidified mesangial matrix. These structures were observed in axial as well as in juxtacapillary mesangial regions (Fig. 6). Occasionally, capillary profiles were seen which were almost totally surrounded by solidified mesangial masses, having lost contact with the GBM. The compact matrix in those areas often contained cross-banded collagenous fibres.

Fig. 7a, b Capillary ballooning. This TEM shows (**a**) glomerular lobule with three expanded superficial capillaries. The lower capillary is associated with a partially retraced mesangium protruding into the vessel lumen (*asterisks*). The upper capillaries are only separated by a thin mesangial layer covered on both sides by endothelium (*arrows*). Note the attenuated podocyte cytoplasm (*arrowheads*) with pseudocyst formation (*star*). **b** Enlargement of the mesangial bridge shown in (**a**). This area represents the outermost part of a mesangium which is in the process of retraction. (**a**) ×1900, (**b**) 4400

These three types of change could be found side by side within the same glomerular lobule. Mixed pictures were also seen; fluid-filled spaces were located within an overall solidified mesangial expansion area, suggesting that acute changes may be superimposed on already solidified chronic lesions. An important feature is that all types of mesangial expansion observed retained a local circumscribed character. Proliferating processes of the mesangium may be prominent locally, but would appear not to be the decisive process leading to segmental sclerosis. We did not find a single glomerulus, in which mesangial proliferation and expansion appeared to result in glomerular destruction.

2. Capillary ballooning/Glomerular microaneurysms

In the majority of tufts in UNX and CON animals the capillary loops appeared fairly uniform in size and small in diameter. In UNX glomeruli, however, we frequently found abnormally shaped capillary loops with remarkably large calibres. They were often seen in clusters in peripheral parts of the tuft (often comprising the first branches of the afferent arteriole) but a more widespread occurrence was also seen. There was a great structural variety in the dilated capillary profiles; Figure 7 shows an example of this kind of capillary ballooning.

The endothelium of even the largest profiles was always intact and exhibited the normal perforated pattern. Discontinuities in the endothelial layer were not observed (Fig. 7). However, local changes in the mesangium were generally seen in association with these ballooned capillaries. In sections where both the ballooned capillary and the corresponding mesangial axis were seen, the mesangium was often found as a coarse agglomeration of cells and matrix protruding into the capillary lumen (the beginning of such a protrusion is seen in Fig. 7).

Dilated capillaries may advance to a glomerular microaneurysm and these were seen in different stages of development: early stages presented as empty holes with only a few platelets and blood cells fixed to the walls. Later stages showed cysts filled with blood derived material in different degrees of thrombus organization.

3. Podocyte lesions

Podocytes showed considerable hypertrophy in the enlarged glomeruli of the DOCA-UNX rat. No signs of podocyte hyperplasia (cell multiplication) were found, but this question was not specifically addressed. The hypertrophied podocytes (Fig. 8) had considerably enlarged cell bodies containing a large nucleus with many indentations. The perinuclear cytoplasm was densely filled with rough endoplasmatic reticulum and Golgi areas. Primary processes often extended to remote capillaries, splitting there into the usual pattern of foot processes.

In areas of lobular expansion (where a lobule or part of a lobule was increased in volume and had lost its nor-

Fig. 8 Podocyte lesions in an area of lobular unfolding. TEM of severely damaged part of a lobule with mesangial lesions (*asterisks*), capillary ballooning (*circles*) and capillary unfolding (note that the uppermost capillary profile lies quite distant from all other profiles). Two hypertrophied podocytes (*1, 2*) are seen which serve quite remote capillary surface (indicated by *arrow-heads* for podocyte *2*). Podocyte damage consists in pseudocyst formation (*stars*) and attenuation of cell bodies (*arrows*); processes are stretched out (*two arrows*). ×1500

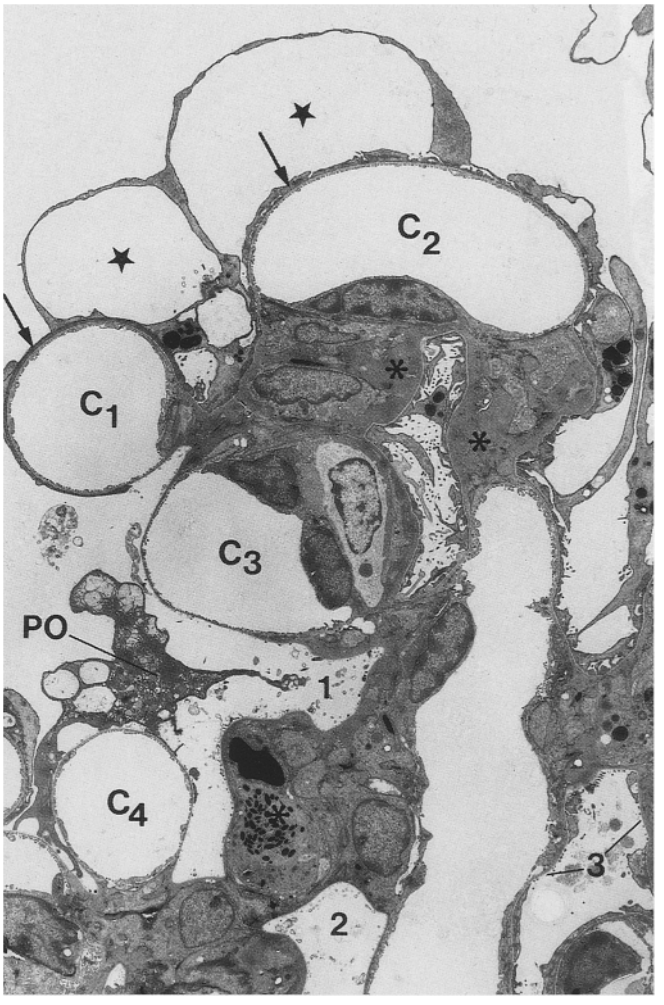

Fig. 9 Podocyte destruction. TEM of expanded lobule associated with severely damaged podocytes and hyalinosis of the mesangium. The podocytes covering the superficial capillaries (*C1, C2*) exhibit pseudocysts (*stars*) and widespread simplification in the foot process pattern (*arrows*). More centrally a dying podocyte (*PO*) is seen, which is in the process of detachment from the GBM at multiple sites. The corresponding capillaries (*C3, C4*) are widely denuded. Naked GBM areas are also seen at various other sites (*1, 2, 3*). The mesangium is partially filled with hyalinized material (*asterisks*). The integrity of the capillaries including their endothelium is maintained. ×1750

mal architecture due to mesangial expansion or capillary ballooning, as described above), podocytes generally exhibited severe degenerative changes (Figs. 3, 7 and 8). The most prominent changes were: cell body attenuation resulting in large, pancake-like cytoplasmic sheets covering extensive parts of the outer capillary surface. The spaces below the cell bodies (subcell body spaces) were thereby dramatically enlarged and narrowed. In these areas multiple pseudocysts were found. In favorable specimens it could be seen, that the floor of a pseudocyst (bleb) may consist of normal filtration barrier with interdigitating foot processes (Fig. 7). Primary processes were frequently stretched and thinned out (best seen by SEM; not shown). Moreover, retraction (fusion) of foot processes was commonly seen. As a consequence the podocytes were attached to the GBM by broad cytoplasmic plaques which contained densely arranged microfilament bundles (Fig. 9).

Detachments of podocytes from the GBM were found in all glomerular profiles that had severe destruction in tuft architecture (Fig. 9). The denudation of the GBM was in some instances a circumscribed distinct lesion consisting of the disappearance of few foot processes, suggesting damage to a single primary process. Extensive denuded areas were also found apparently due to the loss of several podocytes.

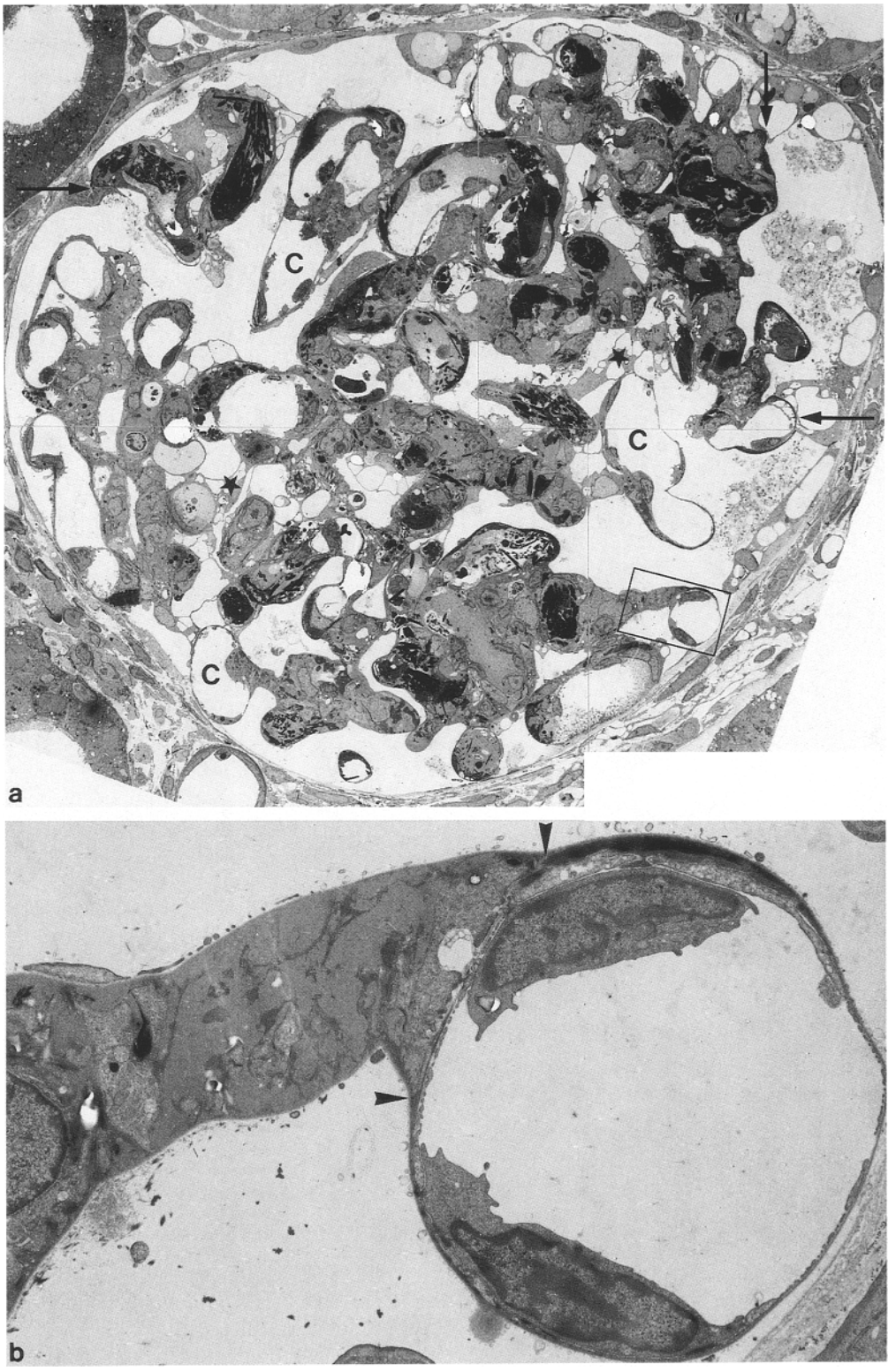

Fig. 10a, b Hyalinosis and tuft appositions/adhesions in a "naked" glomerulus. These TEMs show (**a**) an almost totally denuded glomerulus. The major part of the GBM surface is without any podocyte coverage. Only a few podocytes (*stars*) are left exhibiting severe damage. Excessive hyalinosis of the mesangium is seen. Numerous capillaries are patent (*C*), whereas others are partially or completely filled with thrombi. Several adhesions of denuded peripheral capillaries to parietal epithelial cells or even direct to the basement membrane of the Bowman's capsule are seen (*arrows*). **b** Enlarged area of the quadrangle designated in (**a**). A capillary profile with a narrow "neck" is seen. The severely altered mesangium has an intact juxtacapillary process, which maintains the interconnection of both opposing mesangial angles (*arrowheads*). Note the absence of mesangial proliferation. Note that the capillary architecture is maintained without support from podocytes. (**a**) ×650, (**b**) ×5500

4. Development to sclerosis

The development to sclerosis appears to depend on the localization and extension of podocyte detachments from the GBM. In most severely damaged tufts (Fig. 10) the surface of much of the entire GBM was denuded associated with widespread hyalinosis as well as thrombosis of capillary loops throughout the tuft. Generally, attachments of parietal cells to peripheral capillaries were seen at several sites of the tuft and appeared to develop into adhesions. These lesions progressed to obliteration of capillaries throughout the tuft, ending up in global sclerosis (Fig. 12b).

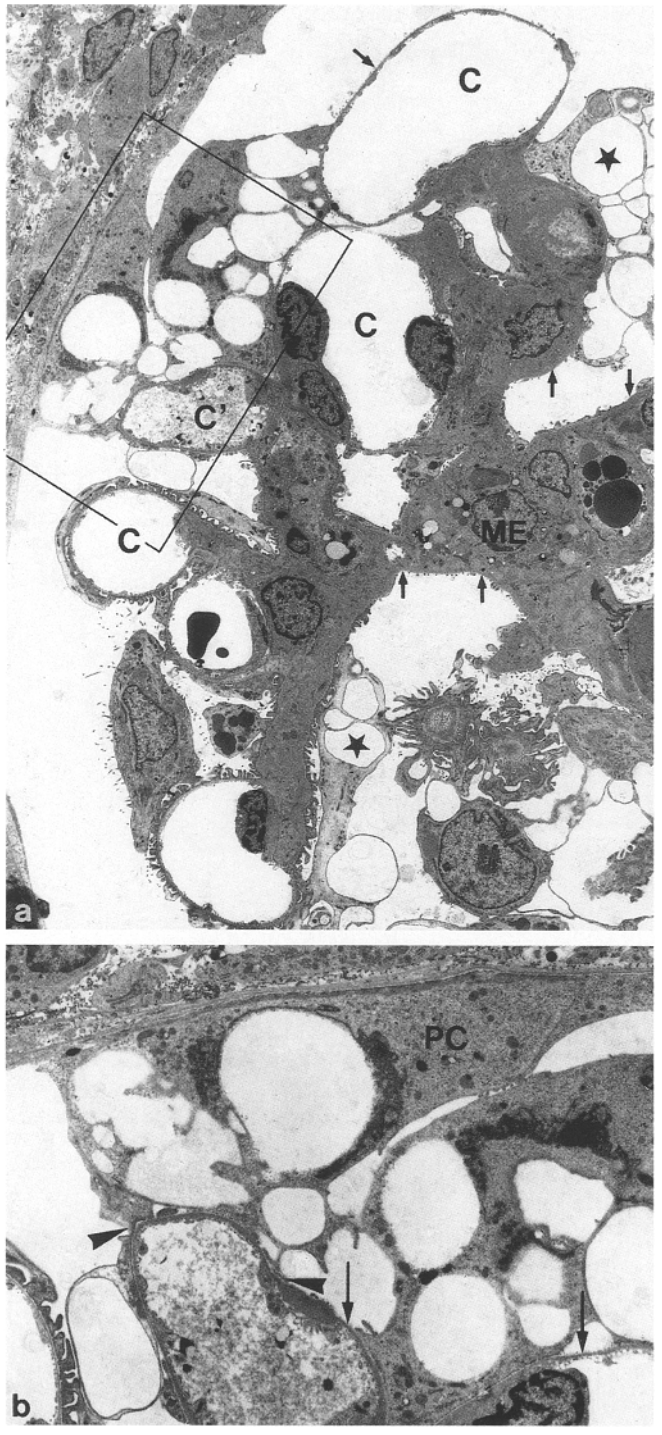

Fig. 11a, b Adhesion follows GBM-denudation. TEM of glomerular lobule in advanced stage of destruction. Areas of severe podocyte lesions (*stars*) alternate with sections of capillaries without any podocyte coverage. Widespread denudations (*arrows*) are found in peripheral as well as in more central parts of the glomerulus. The mesangium is massively expanded (*ME*), at other sites superimposed hyalinosis is found. The majority of the capillaries are patent (*C*) with an intact endothelium, in one capillary (*C'*) the beginning of an obstructive process is visible. The quadrangle in (**a**) is enlarged in (**b**) showing peripheral capillaries with denuded GBM areas (*arrows*). A parietal epithelial (*PC*) cell has gained access to the GBM (*arrowheads*). This is interpreted as a "beachhead" for a synechia formation. (**a**) ×1800, (**b**) ×3800

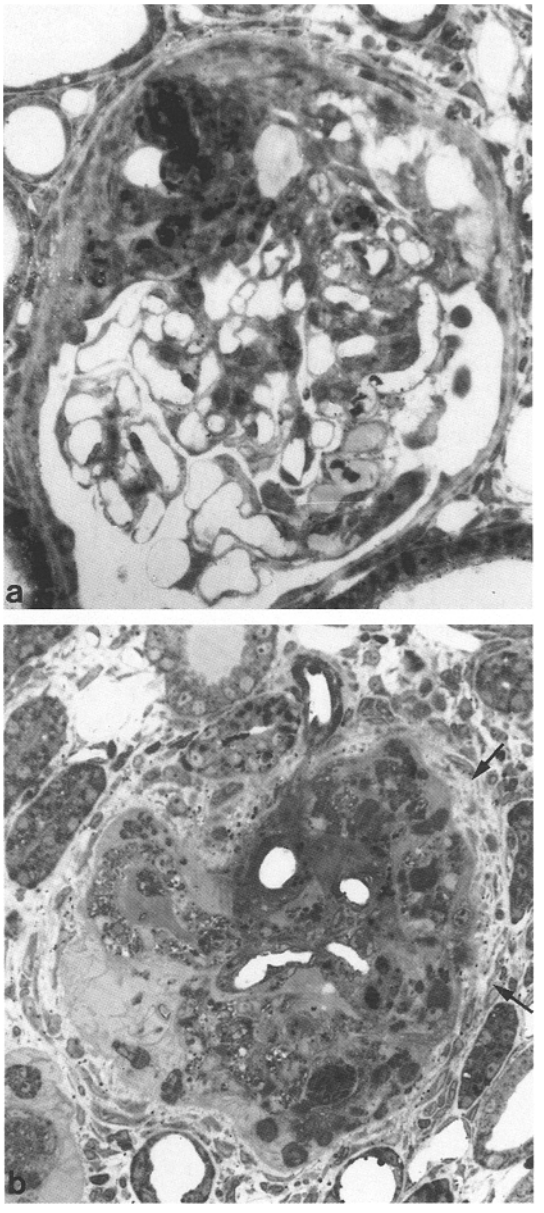

Fig. 12a, b Glomerulosclerosis. **a** Segmental glomerulosclerosis with synechia formation. In the adherent tuft region hyalinosis and thrombosis are seen. **b** Global glomerulosclerosis. The hyalinized tuft contains an open vascular channel, several thrombosed capillaries and is surrounded by periglomerular fibrosis (*arrows*). (**a**) ×440, (**b**) ×380

The more frequent route of sclerosis appeared to start locally with a single tuft adhesion to Bowman's capsule. Such an early adhesion consisted of a single parietal cell attached to the GBM of a peripheral capillary (Fig. 11). More advanced adhesions were associated with hyalinosis and thrombosis leading to capillary obstruction in the adherent tuft region. Those lesions are indicative of segmental sclerosis (Fig. 12a).

Discussion

Compared with previous experiments in the same rat strain which followed a similar protocol [4, 5, 6], our animals showed more severe hypokalaemia (2.66 vs 3.2–3.4 mEq/l), albuminuria (183 mg/day vs a proteinuria of 58–96 mg/day), and greater death rate (3 vs 0). The reason for this difference is not obvious. A higher sensitivity to DOCA [30] in our somewhat younger rats (150–170 g vs 175–200 g) might be a relevant factor.

Glomerular hypertrophy was somewhat less extensive than previously observed. Seven weeks after UNX the increase in VG was about 82% in superficial glomeruli, in juxtamedullary about 52%. After only 4 weeks of study, Dworkin and co-workers [3] found an increase in total glomerular volume (not separated into superficial and deep glomeruli) of about 135%.

Since the hypertrophic growth of juxtamedullary glomeruli was significantly less, the normal size difference between superficial and deep glomeruli (as well as tufts) was totally abolished in the UNX animals (Table 4). Both types of glomeruli stopped growing at a certain size (at about 4×10^6 μm^3 VG). A similar growth pattern was seen by Nagata and co-workers [24] and Iversen and Ofstad [15]; whether this size represents the maximal possible endpoint of hypertrophic growth or whether at this point structural damage starts to supervene, cannot be decided. Glomeruli entering the destructive pathway were all at the upper level of hypertrophy.

Mesangial proliferation associated with increased deposition of mesangial matrix is widely discussed to represent the pathogenetically crucial process in the development of focal and segmental sclerosis [2, 9, 31]. The present study confirms that mesangial expansion is a prominent feature of the UNX-DOCA-model [3].

As shown by direct micropuncture studies, glomeruli in the DOCA-UNX-model are exposed to increased arterial pressures [3, 4] which will result in increased distending forces across the capillary as well as the perimesangial wall. The mesangium is the crucial structure counteracting these forces [35], and the changes seen in the mesangium probably arise as the consequence of an increased mechanical stress to the mesangium [37]. As discussed recently [21, 36] mesangial failure results from insufficiency of the contractile apparatus of mesangial cells, from disruptions of mesangial cell GBM-connections or (in most extreme cases, which are known as mesangiolysis) from cell death and lysis of mesangial matrix.

The local widening and fluid imbibition of the mesangium (as seen in Figs. 4 and 5) may be interpreted as a consequence of recent disruptions of mesangial cell-GBM connections. Widening of the mesangium may lead to increased fluid fluxes through the mesangium bringing mesangial cells into more intensive contact with blood derived growth factors. Moreover, damaged mesangial cells themselves may release growth factors [9]. As a consequence, proliferation of mesangial cells followed by increased matrix production could be induced. These processes could be seen as "aiming" to re-establish the structural stability of the tuft [21] and the result, the solidified mesangial expansion, may be regarded as "successful" repair in the sense, that the GBM has been reattached to the mesangium.

The process of capillary ballooning has recently been analysed in detail [21, 24, 36]. The width of a capillary and its bend form are sustained by centripetal fixation of the GBM to the mesangium. Basically, mechanical failure of the mesangium leads to expansion of the mesangium (as described above), if the mesangial lesions are confined to a limited area. If mechanical failure is more widespread and includes the juxtacapillary region, the loss of capillary support function will cause local ballooning of capillaries. As the mesangial damage proceeds, the process of ballooning impinges upon adjacent capillary loops resulting in unfolding, straightening and ballooning of the involved capillaries.

This failure in capillary support function may also lead to the formation of a glomerular microaneurysm. The hallmark of a glomerular microaneurysm is endothelial damage and merging of capillary and mesangial spaces, but capillary ballooning occurs without disruption of the endothelial layer. Microaneurysms may develop from a ballooned capillary and once established are considered to be a different entity. The development from a microaneurysm to sclerosis is straightforward and has been studied repeatedly [3]. Microaneurysms have been said to be a rare event [34]; in the present study they were found only occasionally (1.2%); their contribution as an initiating mechanism of segmental sclerosis would seem relevant for only a small fraction of glomeruli.

In contrast, capillary ballooning is a frequent event observed in a variety of models [13, 14, 15, 24, 27, 31, 36, 38] and in human autopsies [12]. In our view, capillary ballooning gains considerable pathogenetic relevance via induction of the podocyte lesions.

As has recently been shown in another model of progressive renal disease (UNX in young rats [24]), the local increase in outer capillary surface in addition to overall glomerular hypertrophy may overextend the corresponding podocytes. The typical podocyte lesions – as seen in the present study – are interpreted as maladaptive, as a consequence of inability of this cell to withstand increased mechanical strain due to increased wall tension in ballooned capillaries (according to Laplace's law) and to cope in growth with expanding outer capillary surfaces. Podocytes cover the outer surface of the GBM in a well known pattern of interdigitating foot processes. Any enlargement in GBM surface area challenges the adaptive potential of the corresponding podocytes. Although there is some conflicting evidence [10] most data suggest that the podocyte in the adult kidney has only limited potential for cell division [11, 19, 21, 23, 25, 29]. Thus hypertrophic growth is the only mechanism available to cover the enlarging GBM surfaces.

Podocyte hypertrophy clearly has its limits, thereafter the sequence of maladaptations and lesions –as described

above – begins. Similar lesions have previously been observed in other models of progressive renal disease [3, 8, 13, 23, 26] as well as in human biopsy specimens [1, 43].

Finally, the most serious lesion is the detachment of podocytes from the GBM, an event which may be interpreted as the result of severe overextension. Detachment of podocytes from the GBM – in our view – is the crucial lesion representing the nidus for the final development to sclerosis. Our findings suggest at least two tracks along which the final destruction occurs.

The first pathway to sclerosis starts with widespread denudation of GBM within an entire tuft (Fig. 10). Denuded GBM areas probably have abnormally high hydraulic conductivity [34, 33], allowing a substantially increased filtration at this site. Large serum proteins which cannot pass through the filter even at this damaged sites, may accumulate and precipitate to hyalinosis of the capillary and mesangium. Hyalinosis may subsequently spread over extensive parts of a lobule, frequently associated with microthrombosis contributing to obstruction and collapse of glomerular capillaries [28, 41]. In case that entire tuft is involved as shown in Fig. 10), this stage – without any major proliferating process – appears to progress to a fully developed global sclerosis (as shown in Fig. 12b).

The second pathway involves tuft adhesions to Bowman's capsule starting with a single parietal cell attaching to the GBM of a peripheral capillary (Fig. 11). In the vicinity of those "early" adhesions denuded portions of the GBM were commonly seen. The elaboration of an early adhesion suggests that a denuded portion of the GBM has come into contact with the parietal epithelium allowing the access of a parietal cell to the GBM. This parietal cell then fixes to the GBM and establishes a "beachhead" on the tuft (Fig. 11); other parietal cells will follow.

More advanced stages of an adhesion often show widespread involvement of the parietal epithelium leading to extensive fixation of the tuft to Bowman's capsule. In the related tuft area podocyte detachments from the GBM occur along with the formation of hyalinized foci (hyalinosis) inside the GBM. Again microthrombosis contributes to capillary obstruction. Since these synechial lesions are generally restricted to a single lobule they progress to segmental sclerosis (Fig. 12a).

This development of segmental sclerosis has been previously observed in an ablation model (UNX in young rats [23]) as well as in chronic Masugi nephritis [18]. Denudation of the GBM has been seen in various animal models [11, 17, 22, 34] as well as in human biopsies [1, 12, 43]. Denudation of the GBM, even if localized, must be considered as a serious lesion which may potentially lead to sclerosis.

In the DOCA-UNX model of glomerular hypertension mesangial failure as a consequence of the increased strain on the mesangium-GBM unit plays an important initiating role, leading locally to mesangial, capillary or even lobular expansion. In these regions mesangial proliferation occurs resulting in solidified expanded mesangial areas. However, mesangial proliferation is always a local event; mesangial proliferation as a self-perpetuating process destroying an entire lobule was not encountered. The critical step leading to the irreparable damage of a glomerulus would appear to be the failure of podocytes to cover hypertrophied and expanded tuft areas. Podocytes seem unable to cope with the increased GBM area which results from overall tuft hypertrophy and local tuft expansion. Consequently the podocytes develop severe abnormalities, leading to GBM denudation. Naked GBM areas appear to be the focus for hyalinosis and synechia formation which progress to glomerulosclerosis.

Acknowledgements This study was supported by the Deutsche Forschungsgemeinschaft, Forschergruppe "Niere" Heidelberg. We thank Ms. Hiltraud Hosser, Ms. Bruni Hähnel and Ms. Ingrid Hartmann for their skillful technical assistance. The excellent photographical work by Ms. Ingrid Ertel is gratefully acknowledged. Prof. Dr. P. Röbruck (Institut für Medizinische Biometrie und Informatik, Heidelberg) gave valuable statistical advice, Prof. Dr. T. Unger and Dr. R. Rettig (Pharmakologisches Institut, Heidelberg) showed us how to measure blood pressure in the rat and Prof. Dr. J. Hoyer (Children's Hospital, Philadelphia, USA) provided us with the anti-albumin antibody; their help is gratefully acknowledged. We also thank Dr. Laurie Duncan and Dr. Josie Briggs for a critical review of the manuscript.

References

1. Cohen AH, Mampaso F, Zamboni L (1977) Glomerular podocyte generation in human renal disease. An ultrastructural study. Lab Invest 37:30–42
2. Diamond JR, Karnovsky MJ (1988) Focal and segmental glomerulosclerosis: analogies to atherosclerosis. Kidney Int 33:917–924
3. Dworkin LD, Hostetter TH, Rennke HG, Brenner BM (1984) Hemodynamic basis for glomerular injury in rats with desoxycorticosterone-salt hypertension. J Clin Invest 73:1448–1461
4. Dworkin LD, Feiner HD, Randazzo J (1987) Glomerular hypertension and injury in desoxycorticosterone-salt rats on antihypertensive therapy. Kidney Int 31:718–724
5. Dworkin LD, Feiner HD, Parker M, Randazzo J (1990) Calcium carbonate exacerbates glomerular capillary hypertension and injury in rats with desoxycorticosterone-salt hypertension. Am J Hypertens 3:444–450
6. Dworkin LD, Levin RI, Bernstein JA, Parker M, Ullian ME, Kim Y, Feiner HD (1990) Effects of nifedipine and enalapril on glomerular injury in rats with desoxycorticosterone-salt hypertension. Am J Physiol 259:F598–F604
7. Elger M, Sakai T, Kriz W (1988) Role of mesangial cell contraction in adaptation of the glomerular tuft to changes in extracellular volume. Pfluegers Arch 412:42–53
8. Faraj AH, Morley AR (1993) Remnant kidney pathology after five-sixth nephrectomy in rat. II. Electron microscopy study. APMIS 101:83–90
9. Floege J, Burns MW, Alpers CE, Yoshimura A, Pritzl P, Gordon K, Seifert RA, Bowen-Pope DF, Couser WG, Johnson RJ (1992) Glomerular cell proliferation and PDGF expression precede glomerulosclerosis in the remnant kidney model. Kidney Int 41:297–309
10. Floege J, Johnson RJ, Alpers CE, Fatemi-Nainie, Richardson CA, Gordon K, Couser WG (1993) Visceral glomerular epithelial cells can proliferate in vivo and synthesize platelet-derived growth factor B-chain Am J Pathol 142:637–650

11. Fries JW, Sandstrom DJ, Meyer TW, Rennke HG (1989) Glomerular hypertrophy and epithelial cell injury modulate progressive glomerulosclerosis in the rat. Lab Invest 60:205–218
12. Grishman E, Churg J (1975) Focal glomerular sclerosis in nephrotic patients: An electron microscopic study of glomerular podocytes. Kidney Int 7:111–122
13. Hostetter TH, Olson JL, Rennke HG, Venkatachalam MA, Brenner BM (1981) Hyperfiltration in remnant nephrons: a potentially adverse response to renal ablation. Am J Physiol 241:F85–F93
14. Hostetter TH, Meyer TW, Rennke HG, Brenner BM (1986) Chronic effects of dietary protein in the rat with intact and reduced renal mass. Kidney Int 30:509–517
15. Iversen BM, Ofstad J (1987) The effect of hypertension on glomerular structures and capillary permeability in passive Heymann glomerulonephritis. Microvasc Res 34:137–151
16. Kaissling B, Kriz W (1983) Variability of intercellular spaces between macular densa cells: a transmission electron study in rabbits and rats. Kidney Int 22:9–17
17. Kanwar YS, Rosenzweig LJ (1982) Altered glomerular permeability as a result of focal detachment of the visceral epithelium. Kidney Int 21:565–574
18. Kondo Y, Akikusa B (1982) Chronic Masugi nephritis in the rat. An electron microscopic study on evolution and consequences of glomerular capsular adhesions. Acta Pathol Jpn 32(2):231–242
19. Kriz W, Nagata M, Kretzler M, Koeppen-Hagemann I, Elger M, Lemley K (1994) The role of podocytes in the development of glomerulosclerosis. Kidney Int Suppl 45:S64–S72
20. Lemley KV, Kriz W (1991) Glomerular injury in analbuminemic rats after subtotal nephrectomy. Nephron 59:104–109
21. Lemley KV, Elger M, Koeppen-Hagemann I, Kretzler M, Nagata M, Sakai T, Uiker S, Kriz W (1992) The glomerular mesangium: capillary support function and its failure in experimental conditions. Clin Invest Med 70:843–856
22. Miller P, Scholey JW, Rennke HG, Meyer TW (1990) Glomerular hypertrophy aggravates epithelial cell injury in nephrotic rats. J Clin Invest 85:1119–1126
23. Nagata M, Kriz W (1992) Glomerular damage after uninephrectomy in young rats. II. Mechanical stress on podocytes as a pathway to sclerosis. Kidney Int 42:148–160
24. Nagata M, Schärer K, Kriz W (1992) Glomerular damage after uninephrectomy in young rats. I. Hypertrophy and distortion of capillary architecture. Kidney Int 42:136–147
25. Nagata M, Yamaguchi Y, Ito K (1993) Loss of mitotic activity and the expression of vimentin in glomerular epithelial cells of developing human kidneys. Anat Embryol (Berl) 187:275–279
26. Olson JL, Heptinstall RH (1987) Nonimmunologic mechanisms of glomerular injury. Lab Invest 59:564–578
27. Olson JL, Hostetter TH, Rennke HG, Brenner BM, Venkatachalam MA (1982) Altered glomerular permselectivity and progressive sclerosis following extreme ablation of renal mass. Kidney Int 22:112–126
28. Olson JL, Uradaneta AG, Heptinstall RH (1985) Glomerular hyalinosis and its relation to hyperfiltration. Lab Invest 52:387–398
29. Pabst R, Sterzel RB (1983) Cell renewal of glomerular cell types in normal rats. An autoradiographic analysis. Kidney Int 24:626–631
30. Rascher W (1985) Experimentelle Formen der Hypertonie. In: Ganten D, Ritz E (eds) Lehrbuch der Hypertonie. Schattauer, Stuttgart, pp 51–61
31. Rennke HG (1986) Structural alterations associated with glomerular hyperfiltration. In: Mitch WE (ed) The progressive nature of renal disease. Contemporary Issues in Nephrology. Churchill Livingston, New york, pp 111–131
32. Rennke HG (1994) How does glomerular epithelial cell injury contribute to progressive glomerular damage. Kidney Int Suppl 45:S58–S63
33. Rennke HG, Klein PS (1989) Pathogenesis and significance of nonprimary focal and segmental glomerusclerosis. Am J Kidney Dis 13:443–456
34. Rennke HG, Anderson S, Brenner BM (1989) Structural and functional correlations in the progression of kidney disease. In: Tisher CC, Brenner BM (eds) Renal pathology. Lippincott, Philadelphia, pp 43–66
35. Sakai T, Kriz W (1987) The structural relationship between mesangial cells and basement membrane of the renal glomerulus. Anat Embryol (Berl) 176:373–386
36. Sakai T, Lemley KV, Hackenthal E, Nagata M, Nobiling R, Kriz W (1992) Changes in glomerular structure following acute mesangial failure in the isolated perfused kidney. Kidney Int 41:533–541
37. Schneider U, Inke G, Schneider W, Zahl (1969) Abstand der Verzweigungsstellen vom Rand des Sinus renalis und kaliber der extrarenalen Nierengefäße des Menschen. Anat Anz 124:278–291
38. Schwartz MM, Bidani AK (1991) Mesangial structure and function in the remnant kidney. Kidney Int 40:226–237
39. Shirato I, Sakai T, Fukui M, Tomino Y, Koide H (1993) Widening of capillary neck and alteration of extracellular matrix ultrastructure in diabetic rat glomerulus as revealed by computer morphometry and improved tissue processing. Virchows Arch [A] 423:121–129
40. Sterzel RB, Luft FC, Gao Y, Gao Y, Schnermann J, Briggs JP, Ganten D, Waldherr R, Schnabel E, Kriz W (1988) Renal disease and the development of hypertension in saltsensitive Dahl rats. Kidney Int 33:1119–1129
41. Van Gorh H, Fidler V, Weening JJ, Grond J (1991) Determinants of focal and segmental glomerulosclerosis in the rat after renal ablation. Evidence for involvement of macrophages and lipids. Lab Invest 64:754–765
42. Weibel ER (1979) Stereological methods. Practical methods for biological morphometry. Academic Press, London
43. Yoshikawa N, Hiroshi I, Akamatsu R, Hazikano H, Okada S, Matsuo T (1986) Glomerular podocyte vacuolation in focal segmental glomerulosclerosis. Arch Pathol Lab Med 110:394–398